Journal of The Electrochemical Society, **156** (1) B51-B58 (2009)
0013-4651/2009/156(1)/B51/8/$23.00 © The Electrochemical Society

Well-Alloyed PtFe/C Nanocatalysts of Controlled Composition and Same Particle Size: Oxygen Reduction and Methanol Tolerance

Arthur R. Malheiro,* Joelma Perez,* and H. Mercedes Villullas,z**

Departamento de Físico Química, Instituto de Química, Universidade Estadual Paulista (UNESP), 14801-970 CP 355, Araraquara (SP), Brazil

A study of the effect of iron concentration on the electrocatalysis of oxygen reduction reaction (ORR) on well-alloyed carbon-supported PtFe nanocatalysts with a controlled iron content and the same particle size is presented. To obtain the catalysts for this study, PtFe nanoparticles of different compositions were first obtained in a colloidal state in sodium bis(2-ethylhexyl)sulfosuccinate (AOT)+*n*-butanol/*n*-heptane/water microemulsions and subsequently supported in high surface area carbon powder. Transmission electron microscopy evidenced that all PtFe/C nanocatalysts prepared are monodispersed and have nearly the same average particle size. X-ray diffraction studies showed that the lattice parameter of these PtFe/C catalysts varies linearly with iron content up to 50% (in atoms), while the compositions of the alloyed phases estimated by using Vegard's law are almost identical to the nominal values, indicating a high degree of alloying. The electrocatalytic activity for ORR of these catalysts was studied using the rotating disk electrode technique in O_2 saturated 0.5 mol L^{-1} H_2SO_4 solutions, while methanol tolerance was evaluated from curves taken in acid solutions containing 0.1 mol L^{-1} methanol. The results reported here reflect the dependence of the electrocatalytic activity for the ORR on iron concentration in the absence of particle size effects and metal segregation.
 [DOI: 10.1149/1.3006082]

Manuscript submitted August 12, 2008; revised manuscript received October 2, 2008. Published November 4, 2008.

The growing awareness of the risks related to human-induced climate change has considerably raised the necessity of alternative ways of energy production. In this context, the conversion of chemical energy into electricity has become increasingly important and, thus, clean and efficient devices such as fuel cells are now attracting a great deal of attention from governments, academic institutions, and private businesses. While fuel cells might help to overcome the power problems, there are still a number of issues to be worked out to make the generation of electrical power using fuel cells practical and cost-effective.

Among the different fuel cell types, the proton exchange membrane fuel cell (PEMFC) is considered the most adequate for vehicle and portable applications. However, much needs to be done to improve the performance. Among other problems, the slow kinetics of the oxygen reduction reaction (ORR) remains one of the key factors affecting the performance of PEMFCs, causing overpotential losses of ~0.3 to 0.4 V under typical operation conditions.[1] To tackle this problem, electrocatalysts more efficient than Pt are required. Aiming to reduce the voltage losses associated with the cathode performance, a number of Pt-based bimetallic systems, such as Pt–Fe,[2-15] Pt–Mn,[2] Pt–Cu,[5,9] Pt–Ni,[2,4,5,9,14-23] Pt–Co,[2,4,5,8-10,14,21-33] Pt–Cr,[2,14,23,33-38] and Pt–V,[14,39,40] have been investigated and, in many cases, catalytic activities for ORR about 1.5–3 times higher than that of pure Pt were reported. Moreover, the use of a second element more abundant than Pt could contribute to reduce the costs of the electrocatalysts.

Toda et al.[3] reported a significant enhancement of electrocatalytic activity for ORR of thin layers of sputter-deposited PtFe alloys with a maximum activity at ca. 50% Fe content. That work was followed by papers dealing with different methods of preparation of carbon-supported PtFe catalysts. Some authors have used the alloying method,[5,6,9-12] which involves depositing the M precursor on Pt/C followed by alloying at high temperature (usually above 700°C), despite the obvious disadvantage of producing a significant increase of average particle size due to sintering of the particles during the thermal treatment. Other techniques such as synthesis in microemulsions,[10] impregnation,[12,13] polyol synthesis,[7,14] and Bönnemann's method[15] were also used to prepare carbon-supported PtFe catalysts.

Despite the fact that a number of studies of ORR on PtFe/C materials have been published, the effects of iron concentration have not been yet properly assessed. In only two reports the ORR was studied on a catalysts of three different compositions.[12,15] In one of them the particle size of the catalysts was not reported,[12] while in the other one the actual iron concentration was not given.[15] In all the other studies catalysts of a single nominal composition, either Pt:Fe 1:1 or Pt:Fe 3:1, were investigated. In general, published results are very difficult to compare, not only for the different conditions in which ORR data were taken, but also because catalysts properties were very different as well. For instance, particle sizes varied greatly among the different works, ranging from 2.8 to 11 nm, actual Fe contents were significantly different from nominal values or not determined, while in many cases thermal treatments were used to promote reduction of the precursors or alloying. Literature results for ORR on carbon-supported PtFe catalysts are summarized in Table I.

In general, published data for PtFe/C catalysts, as well as most data for ORR on PtM/C materials,[41] clearly indicate that properties such as particle size, size distribution, degree of alloying, and actual composition depend on the synthesis conditions.

In a previous study of the ORR on PtFe/C catalysts, we tried to establish the effects of iron concentration for catalysts prepared in sodium bis(2-ethylhexyl)sulfosuccinate (AOT)/*n*-heptane/water microemulsions.[42] Even though the results obtained revealed that catalyst composition influences the kinetics of the ORR, the concentrations of Fe in the catalysts were lower than those attempted in the preparation. Aiming to overcome that problem, a study using the pseudoternary AOT + *n*-butanol/*n*-heptane/water system (at a mass ratio of AOT/*n*-butanol = 2) was recently carried out in our laboratory,[43] and demonstrated that the presence of *n*-butanol in the microemulsion led to the complete reduction of the Fe ions that allowed for obtaining well-alloyed PtFe nanoparticles with the desired composition, without the need of preparing functionalized surfactants or the use of an inert atmosphere. The larger incorporation of Fe observed for nanoparticles prepared in the presence of *n*-butanol as a cosurfactant was interpreted in terms of an increase of the rigidity of the micellar interface, associated with the solubilization of the alcohol in the surfactant tail region that pushes the surfactant head groups together, without significantly altering the size of the water droplets. In that work, it was also shown that it is possible to obtain monodispersed PtFe nanoparticles whose alloyed phase composition was nearly identical to the atomic ratio of the

* Electrochemical Society Student Member.
** Electrochemical Society Active Member.
z E-mail: mercedes@iq.unesp.br

Table I. Published data on physical properties and ORR activity for carbon-supported PtFe catalysts.

					ORR			
Preparation method and metal/C wt %	Nominal composition	Actual composition	Particle size (nm)	Lattice constant (nm)	Mass activity (mA/mg)	Specific activity	Measurements	Ref.
Impregnation					*i* at 0.09 V[a]	*jo* (mA/cm^2)	Galvanostatic	5
(Pt/C 20 wt %)	50:50	72:28	3.7	—	—	—	polarization	
	1:5	—	—	—	97	3.04×10^{-7}	0.5 mol L^{-1} H_2SO_4	
	Pt/C	—	4.8	—	52	1.33×10^{-6}	25°C	
Alloying-750°C						*ik* at 0.8 V (mA/cm^2)	PEMFC-85°C	6
(20 wt % metal/C)	50:50	54:46	11	a = 3.852; c = 3.713	—	297	1.37 mg Pt/cm^2	
	Pt/C	—	3	3.923	—	57		
Ethylene glycol					*ik* at 0.9 V	*ik* at 0.9 V (mA/m^2 Pt)	RDE	7
Heat-treated 300°C	3:1	93:7	3.4	3.912	21.5	341	1 mol L^{-1} $HClO_4$	
Heat-treated 900°C	3:1	—	5.1	3.908	5.4	176	5 mV/s	
Alloying 900°C	3:1	79:21	7.3	3.892	4.1	288	Room temperature	
(Pt/C 20 wt %)	Pt/C	—	2.9	3.927	9.3	137		
Colloidal "sol"						*ik* at 0.9 V (mA/cm^2)[d]	RDE	8
+reduction at 900°C	3:1	79:31[b]	3.9[c]	3.866	—	0.085; 0.033	1 and 6 mol L^{-1}	
(20 wt % metal/C)	Pt/C	—	2.5[c]/	3.927	—	0.057; 0.122	CF_3SO_3H	
Impregnation						*j* at 0.85 V (mA/cm^2)	PEMFC 72°C	9
+heating at 900°C	1:1	Close to 1:1	6.2	a = 3.848; c = 3.7022	—	33	0.3 mg/cm^2	
(Pt/C 20 wt %)	Pt/C	—	3.8	3.921	—	24	(Pt or PtM)	
Microemulsion					*i* at 0.85 V	*j* at 0.85 V (mA/cm^2)	PEMFC-75°C	10
As-prepared	80:20 (wt %)[e]	70:30 (wt %)	2.5[c]	—	110.3	16	Galvanostatic	
Heat-treated 200°C		—	—	—	282	42	loading 0.3 mg/cm^2	
Alloying-900°C		74:26 (wt %)	6.3[c]	—	198	33	(Pt or PtM)	
(Pt/C 20 wt %)	80:20 (wt %)[e] Pt/C	—	3.8[c]	—	82	24		
Impregnation-750°C					*i* at 0.4 V[a]		Steady-state	12
(metal/C wt % not given)	3.8:1	3.74:0.98	—	3.828	80.3	—	polarization	
	1.2:1	2.35:1.95	—	3.815	81.2	—	0.5 mol L^{-1} H_2SO_4	
	1:2.7	2.86:7.71	—	3.835	89.9	—	18°C	
	Pt/C	—	—	3.928	76.8	—		
PtO_x/C Impregnation+						*jo* at 60°C (mA/cm^2)	RDE	13
H_2 (room temperature)	3:1	—	2.4	3.90	—	2.15×10^{-4}	0.5 mol L^{-1} H_2SO_4	
(60 wt % Pt–Fe/C)	Pt/C	3.33:1	2.8	3.92	—	1.63×10^{-5}	5 mV/s; 25–60°C	
Polyol						*jk* at 0.8 V (mA/cm^2)	Channel flow	14
29.4 wt % (Pt–Fe/C)	50:50	50:50	2.1	3.85	—	1.10	0.1 mol L^{-1} $HClO_4$	
24.5 wt % (Pt/C)	Pt/C	—	2.3	3.93	—	0.82	0.5 mV/s; 30°C	
Bönnemann						*j* at 0.40 V (mA/cm^2)	RDE	15
+350°C	1:1	—	2.6	3.89	—	3.95	1 mol L^{-1} $HClO_4$	
(20 wt % metal/C)	3:1	—	3.0	3.89	—	2.76	5 mV/s	
	9:1	—	3.2	3.89	—	3.97	Room temperature	
	Pt/C	—	—	3.92	—	1.70		

[a] Potential vs Hg/Hg_2SO_4.
[b] From in situ XANES measurements.
[c] From XRD analysis.
[d] Values in CF_3SO_3H 1 and 6 mol L^{-1}, respectively.
[e] Corresponds to nearly Pt:Fe 50:50 in atoms.

metals in the aqueous solution of the precursors and that are very well alloyed without the need of any thermal treatment. It was also found that the addition of *n*-butanol as a cosurfactant does not affect the particle size, which continues to be determined by the surfactant to water molar ratio.[43]

Therefore, pseudoternary AOT + *n*-butanol/*n*-heptane/water microemulsions were used in the present work to prepared well-alloyed PtFe/C catalysts with different iron concentrations, monodispersed and with the same particle size. The catalysts were characterized and used to investigate the electrocatalytic activity toward ORR and methanol tolerance as a function of iron concentration in the absence of second metal segregation and particle size effects.

Experimental

PtFe/C nanocatalysts preparation.— PtFe/C electrocatalysts were synthesized by a reverse microemulsion method using AOT as

the surfactant and *n*-heptane as oil phase, with *n*-butanol as the cosurfactant, as described elsewhere.[43] Briefly, the microemulsions were prepared using a weight ratio of *n*-butanol to AOT of 0.5. Aqueous solutions of H_2PtCl_6 and $FeCl_3$ were used to form the reverse micelles by adding the aqueous solution of the precursors to a mixture of *n*-heptane and AOT (15 wt %) under constant stirring for 2 h. In all cases, the water/AOT molar ratio was kept constant ($w = 8$) to obtain particles of the same sizes. The reducing agent ($NaBH_4$) was added to the microemulsion as a solid in a molar ratio of 10:1 to metals. To ensure complete reduction the mixture was kept under constant stirring for 2 h. A series of catalysts with different compositions was prepared, varying the atomic ratio of metal precursors in the aqueous phase. The iron content was varied from 10 to 50% (in atoms). After the nanoparticles were obtained, an adequate amount of high surface area carbon (Vulcan XC-72, Cabot) was then added to the mixture to give a metal loading (Pt + Fe) of 20 wt %. After a short period of ultrasonic treatment, the mixture was kept under constant stirring overnight. The supported catalysts obtained were then filtered, washed copiously with ethanol, acetone, and water, and dried. A completely colorless supernantant, which remained colorless upon the addition of concentrated NH_4SCN solution, served as an indication of complete reduction of the iron, as described elsewhere.[43] For comparison purposes, a Pt/C catalyst was also synthesized and a commercial sample of Pt/C (20 wt %, E-TEK) was used as a control.

Physical characterization techniques.— All catalysts were characterized by X-ray diffraction (XRD) using a Rigaku, model D Max 2500 PC diffractometer using Cu Kα radiation (λ = 1.5406 Å). Scans were done at 0.5° min^{-1} for 2θ values between 10 and 100°. The transmission electronic microscopy (TEM) study was done using a Philips CM 200 microscope operating at 200 kV, coupled to an energy dispersive X-ray analysis (EDX) spectrometer. The samples for the TEM analysis were prepared by ultrasonically dispersing the catalyst powders in ethanol. A drop of the suspension was applied onto a carbon-coated copper grid and dried in air.

Electrochemical characterization.— All the electrochemical measurements were done in a conventional electrochemical cell, with a Pt wire counter electrode placed in a separate compartment and a reversible hydrogen reference electrode. The PtFe/C electrocatalysts were used as ultrathin layers[44] on a glassy carbon (CG) disk electrode (0.196 cm^2) previously polished down to 0.3 μm alumina. In all cases, the catalyst ultrathin layer had a metal load (Pt or PtFe) of 28 μg cm^{-2}. The general electrochemical behavior was characterized by cyclic voltammetry (CV) in N_2-saturated 0.5 mol L^{-1} H_2SO_4. Measurements of electrocatalytic activity for the ORR were done using the rotating disk electrode (RDE) technique in O_2-saturated solution. The methanol tolerance was evaluated through measurements of the ORR in O_2-saturated 0.5 mol L^{-1} H_2SO_4 solution containing methanol in a concentration of 0.1 mol L^{-1}. Solutions were prepared from analytical grade H_2SO_4 (Mallinckrodt), analytical grade methanol (Mallinckrodt), and ultrapure water (MilliQ, Millipore). All experiments were done at 25°C.

Results and Discussion

Physical characterization.— The structural properties of the PtFe/C catalysts were examined by XRD. Figure 1 shows that the XRD patterns of the PtFe/C materials prepared exhibit diffraction signals associated with the face-centered cubic (fcc) Pt structure (PDF 4-802). For all PtFe/C catalysts diffraction peaks are broad and shifted toward higher 2θ values compared to those of Pt/C. This shift in peak position can be taken as a first indication of alloy formation because partial substitution of Pt by Fe in the fcc structure produces a contraction of the lattice.

From the XRD data, the lattice parameter

$$a = \frac{\sqrt{2}\lambda}{\sin\theta} \qquad [1]$$

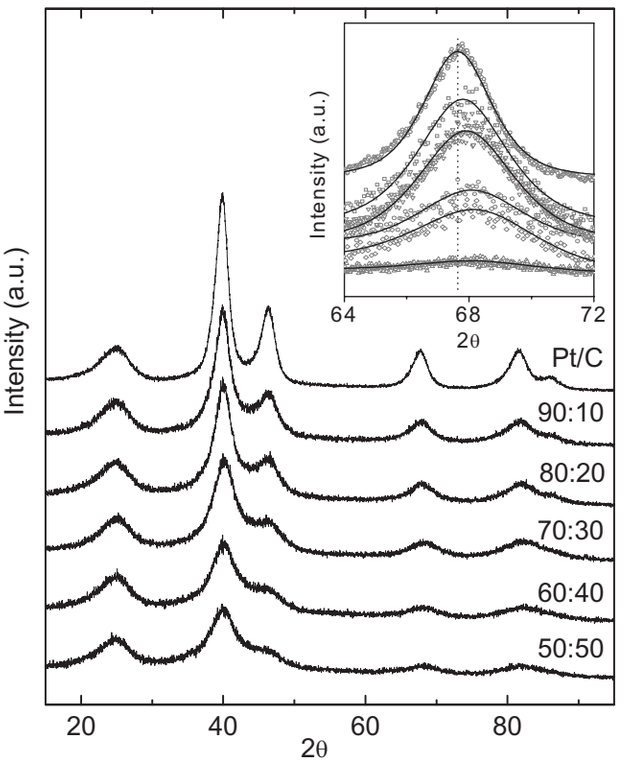

Figure 1. XRD patterns of PtFe/C nanocatalysts (Pt:Fe nominal compositions indicated in the figure). Pattern for Pt/C catalyst is included for comparison. Insert: Pseudo-Voigt fitting of [220] diffraction peaks. The line indicates the [220] peak position of the Pt/C sample.

and the Pt–Pt distance

$$d_{fcc} = \frac{\sqrt{2}}{2}a \qquad [2]$$

at [220] diffraction[15] were also calculated for the PtFe/C catalysts. The values of the lattice constant obtained for the PtFe/C catalysts are smaller than for Pt and decrease as the Fe content of the catalysts increases, as shown in Fig. 2, indicating the incorporation of Fe into an alloyed phase. The linear dependence of the lattice parameter

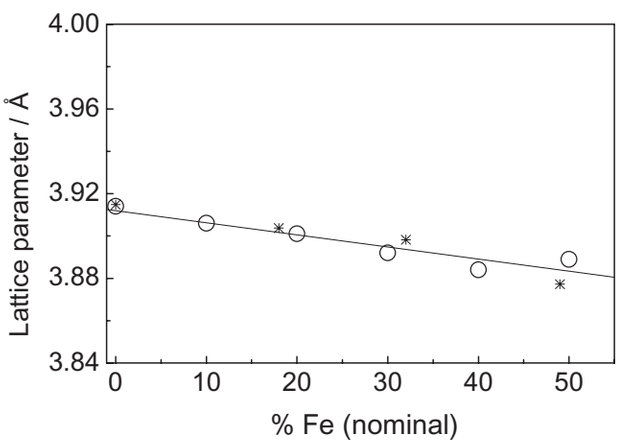

Figure 2. Lattice parameter of PtFe/C nanocatalysts as a function of nominal Fe content (○). Data for PtFe sputtered alloys[3] are included for comparison (∗).

Table II. XRD derived structural characteristics of the PtFe/C and Pt/C nanocatalysts.

Pt:Fe (nominal)	Lattice parameter (Å)	Pt–Pt distance (Å)	x(Fe)	Pt:Fe (alloyed phase)
100:0	3.914	2.786	—	—
90:10	3.906	2.762	0.245	88:12
80:20	3.901	2.758	0.386	81:19
70:30	3.892	2.752	0.605	70:30
60:40	3.884	2.746	0.827	59:41
50:50	3.889	2.749	0.716	64:36

with the iron content indicates that these catalysts obey Vegard's law[45]

$$x_{(\mathrm{Fe})} = \frac{a - a_o}{a_{\mathrm{alloy}} - a_o} \quad [3]$$

where a is the lattice parameter of the PtFe catalyst that depends on composition, a_{alloy} is the lattice parameter for a PtFe solid solution, and a_o is the lattice parameter of Pt. The results shown in Fig. 2 are in excellent agreement with those published by Toda et al.[3] for PtFe sputtered alloys. They observed a nearly linear variation of the lattice constant with the alloy Fe content, revealing that the formation of the chemically disordered fcc structure (solid solution) occurs up to ca. 75% iron content. The fraction of alloyed Fe was calculated for the PtFe/C catalysts taking the lattice parameter for a PtFe solid solution a_{alloy} as 3.877 Å (PDF 29-717). The value of a_o was determined for carbon-supported Pt, 3.914 Å, and found to be in good agreement with literature data.[46] XRD results are summarized in Table II. In a general manner, the lattice parameter and the Pt–Pt distance decrease as the content of Fe increases. Because the values of the actual composition, as determined by EDX analysis, were very close to the nominal compositions attempted in the preparation, the values of $x_{(\mathrm{Fe})}$ obtained show that the composition of the alloyed phase is practically identical to the nominal value, indicating that Fe is in metallic form and well-alloyed with Pt. A slight deviation (lesser incorporation of iron into the alloyed phase) was observed for the sample of nominal composition 50:50, which might be the result of a disruption of the micellar interface caused by the larger amount of Fe ions in the solution.[43]

Figure 3 shows a typical TEM image and a histogram of particle size distribution. For all the PtFe/C catalysts, PtFe nanoparticles were homogeneously distributed on the carbon support. Very narrow particle size distributions were observed, indicating that the PtFe nanoparticles obtained are monodispersed (σ = 11–14%).[47] TEM results also evidenced that the PtFe/C catalysts of different compositions prepared in this work have nearly the same particle size (around 3 nm), as expected from the fact that all samples were prepared using the same water/surfactant molar ratio (w = 8).[43] The results of the TEM characterization of PtFe/C nanocatalysts of different compositions are presented in Table III. Slightly larger values of average particle size and polydispersity were obtained for the Pt/C (3.6 nm and σ = 16%). While the particle size for the 20% Pt/C commercial catalyst used as control was not determined in this study, particle sizes between 2.5 and 4.0 nm[48] and of 3.4 ± 1.2 nm[49] have been previously reported.

Electrochemical behavior and electrocatalysis of the ORR.— The electrochemical properties of PtFe/C nanocatalysts of different compositions were first examined by CV. The curves obtained in N_2 saturated 0.5 mol L^{-1} H_2SO_4, at 50 mV s^{-1} in the potential range of 0.05–0.8 V, are shown in Fig. 4a for electrodes containing the same total amount of metals (28 μg cm^{-2} of PtFe). In all cases, stable profiles were obtained after a few cycles and remained nearly unchanged even after a large number of cycles (>100) up to 1 V. The general features of the voltammetric curves are similar, while the total charges involved in the current–potential curves depend on the

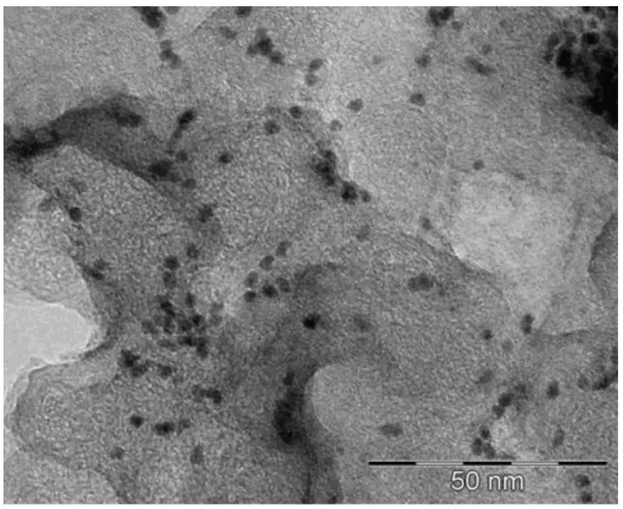

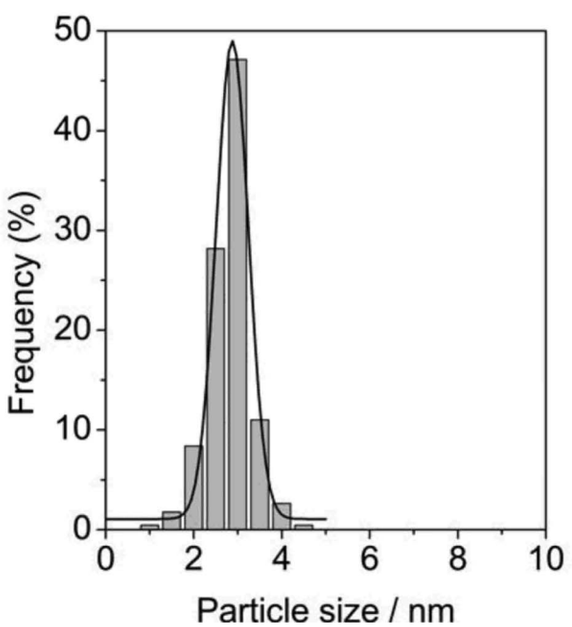

Figure 3. TEM image and particle size histogram for the PtFe/C nanocatalyst of nominal composition Pt:Fe 50:50.

sample composition, and decrease as the Fe content increases. The hydrogen desorption charges were integrated, after accounting for the double-layer contribution, in the same manner as usually done for Pt/C and for PtM catalysts (M = Fe, V, Ni, Co, and Cr),[14] and the results are depicted against the catalysts Fe content in Fig. 4b.

Table III. Results of the TEM study of the PtFe/C nanocatalysts of different compositions.

Pt:Fe (nominal)	TEM particle size (nm)	SD (nm)	σ (%)
90:10	3.3	0.44	13
80:20	3.3	0.37	11
70:30	3.0	0.43	14
60:40	3.3	0.35	11
50:50	2.9	0.39	13

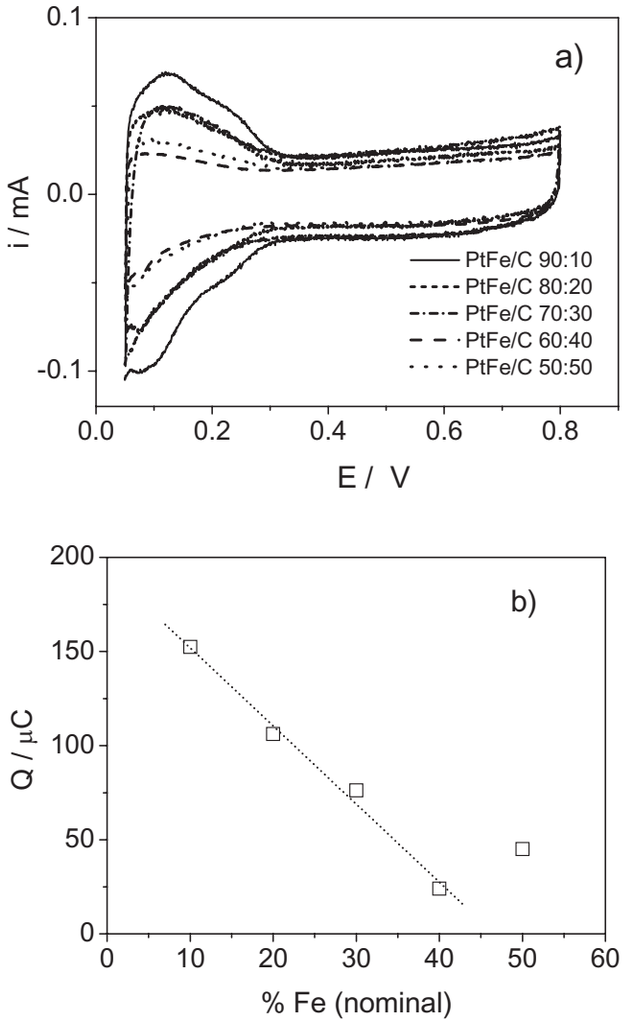

Figure 4. (a) CV curves (fifth cycle) of the PtFe/C nanocatalysts obtained at 50 mV s^{-1} in N_2-saturated 0.5 mol L^{-1} H_2SO_4. (b) Hydrogen desorption charge against nominal Fe content (in atoms).

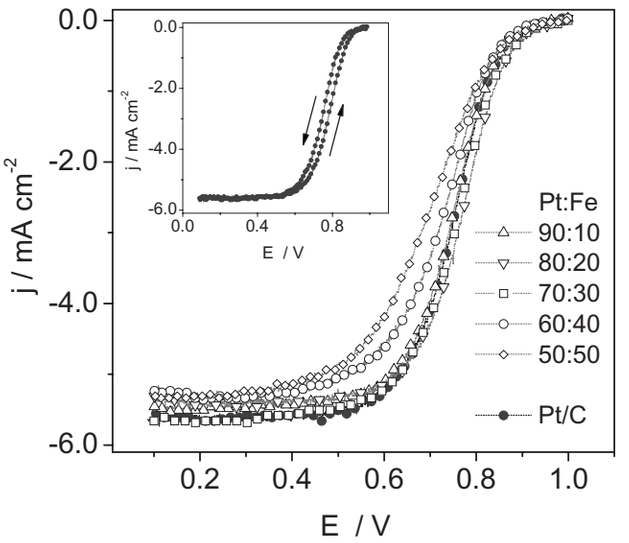

Figure 5. ORR polarization curves of the PtFe/C (negative-going sweeps). All data were obtained in O_2-saturated 0.5 mol L^{-1} H_2SO_4 acid. Rotation rate: 2500 rpm. Inset:ORR negative and positive-going sweeps at 2500 rpm for Pt/C.

Some authors have suggested that the enhanced activity for ORR on bimetallic surfaces may arise from the formation of a Pt skin.[3,4,16] From extended X-ray absorption fine structure studies, Teliska et al.[11] concluded that, while the Pt–Fe and Pt–Cr samples have a Pt skin, Pt–Ni and Pt–Co clusters were more homogeneous with M atoms on the surface. Because all PtFe/C catalysts used in the present study have the same particle size, the formation of a Pt skin should result in similar voltammetric charges. In contrast, the charge associated with the oxidation of adsorbed hydrogen depends on the catalyst's Fe concentration, as shown in Fig. 4b. Because it is known that adsorption of underpotential deposited hydrogen on Fe is inhibited by the presence of oxide species,[50] Fig. 4b indicates that both Pt and Fe are present on the surface in amounts that follow the nominal composition of the nanocatalysts.

A typical set of polarization curves for the ORR on PtFe/C catalysts of different compositions is shown in Fig. 5, where current densities are normalized to the geometric area of the GC substrate. A curve for the Pt/C catalyst is included for comparison. The reaction is diffusion-controlled at potentials below ca. 0.7 V and is under mixed diffusion-kinetic control between ca. 0.70 and 0.95 V. For all catalysts studied, a linear dependence of the limiting diffusion current on the square root of the rotation rate was verified.[51] Moreover, all Levich plots (i_L vs $\omega^{1/2}$) fall together, exhibiting the same slope and a small positive intercept caused by oxygen diffusion within the ultrathin catalyst layer.[52] Even though it is shown only for the Pt/C catalysts (inset of Fig. 5), currents measured in the negative-going sweeps were always lower than in the positive-going direction for potentials above ca. 0.6 V. This hysteresis has also been observed for carbon-supported catalysts[52] and attributed to the effects of the presence of Pt surface oxides in the negative-going potential scan.

The composition of PtFe/C nanocatalysts has a clear influence on the catalytic activity for ORR as evidenced by the mass-transport corrected current densities at 0.90 V shown in Fig. 6a. The values obtained are, in general terms, in very good agreement with literature data (see Table I). The value obtained for the Pt/C commercial sample used as control has also been included. As can be seen, the currents measured for the PtFe/C nanocatalysts of compositions Pt:Fe 90:10, 60:40, and 50:50 are similar to that measured on Pt/C. In contrast, significantly larger currents were measured on the catalysts of composition 70:30 and 80:20. To make an adequate analysis of these results, it should be kept in mind that the metal load (Pt + Fe) in the catalyst layers was kept constant and, therefore, the actual Pt mass on the ultrathin layer electrode decreases as the Fe content of the sample increases. Mass activities obtained by normalization of the kinetic currents by the Pt load are shown in Fig. 6b. It seems quite clear that the mass activity for ORR of all PtFe/C nanocatalysts studied is superior to that of Pt/C.

For all PtFe/C nanocatalysts, mass-transport corrected Tafel plots show a linear region with a Tafel slope close to −60 mV/dec in the region of low overpotentials, followed by a change in the slope to nearly −120 mV/dec for high overpotentials, as shown in Fig. 7 for the catalysts of nominal composition Pt:Fe 80:20. The change of Tafel slope from −60 to − 120 mV/dec is well-known for ORR on polycrystalline Pt,[53] Pt single crystals,[54] carbon-supported Pt catalysts,[51,52] Pt-based catalysts, such as PtFe/C[13] and PtNi/C,[55] and it can be interpreted as caused by changes in the coverage of adsorbed oxygen. At low currents, the coverage of adsorbed oxygen would be high and follow a Temkin isotherm, while for high currents it would be low and follow a Langmuir isotherm. Because Tafel slopes have similar values, the rate-determining step is likely to be the same for all PtFe/C catalysts, despite the dependence of the measured ORR current on Fe content.

As pointed out above and shown in Table I, even though the ORR has been previously studied on PtFe/C catalysts, particle sizes

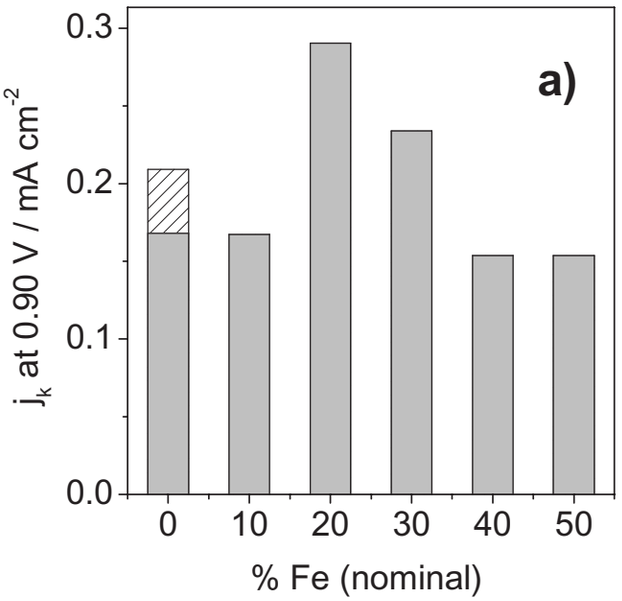

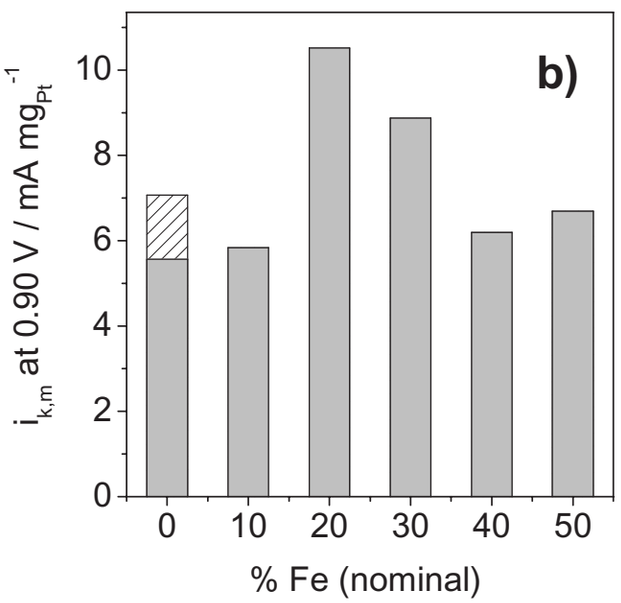

Figure 6. (a) Kinetic current densities of ORR at 0.90 V against Fe nominal content (in atoms). (b) Pt mass-normalized ORR kinetic current densities at 0.90 V. Rotation rate: 2500 rpm.

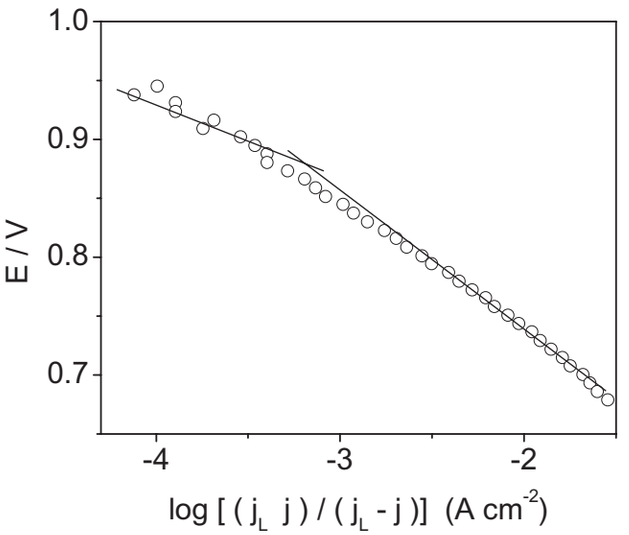

Figure 7. Mass-transfer corrected Tafel plot for ORR on PtFe/C of nominal composition Pt:Fe 80:20.

varied greatly among the different published works. Despite the many questions regarding the influence of catalyst properties on catalytic activity that remained to be answered, there is a general consensus about the influence that particle size might have on the kinetics of the ORR. For instance, the mass activity of Pt in phosphoric acid shows a maximum at d = 3.5 nm, coincident with the maximum of the mass-averaged distribution for the (100) planes.[56,57] In addition, studying carbon-supported Pt-based binary catalysts (PtCo, PtCr, and PtNi), Min et al.[23] concluded that particle size and alloying are the two most important factors affecting the catalytic activity toward ORR. Studies of the ORR on PtCo/C catalysts led Antolini et al.[30] to conclude that the activity of their catalysts could not be explained in terms of either Co content, Pt–Pt distance, or as a function of particle size, pointing out the mutual influence among these parameters. In this context, it is relevant to stress that the most important aspect of the iron concentration screening presented above is that all PtFe/C catalysts studied are well-alloyed and have nearly the same average particle size and very narrow size distributions. The data presented in this work establish composition effects on the kinetics of the ORR in the absence of particle size effects and second metal segregation.

It is generally accepted that the rate-determining step of the ORR is the first electron transfer that occurs either after or simultaneously with the adsorption of O_2.[58] Thus, the electrocatalytic activity for ORR should depend on the amount of Pt sites available for the adsorption of molecular oxygen and on the energy of adsorption of oxygen and reactive intermediates. As mentioned above, enhancement of activity for ORR caused by alloying Pt with 3d transition metals has been observed for several different PtM systems and a variety of possible explanations have been considered. Studying various platinum alloys, Jalan and Taylor[59] proposed that the Pt–Pt nearest-neighbor distance was the main factor affecting the catalytic activity for ORR. Data presented in Table II indicate that the variations of Pt–Pt distance follow up well the changes in iron concentration but do not seem large enough to explain the significant differences in activity shown in Fig. 5-7.

Adsorption of OH species can also inhibit the ORR by blocking surface sites and through electronic effects.[60] Paulus et al.[21] have suggested that, for bimetallic particles with metal M atoms present at the surface, OH species would adsorb at lower potentials onto the more reactive M atoms at the surface and, thus, lateral interactions would prevent adsorption of other OH groups on the surface Pt atoms. The effect of alloying on OH adsorption on the PtM surface (M = Ni, Co, Fe, and Cr) was also examined by Teliska et al.,[11] and the OH inhibition was correlated with kinetic reactivity in fuel cell experiments with those bimetallic materials. These authors concluded that OH inhibition on PtCo and PtNi catalysts would be due to lateral interaction, while their X-ray absorption near-edge structure (XANES) data indicate that electronic effects were dominant on PtFe and PtCr. The dependence of H adsorption/desorption charges on the Fe content of the catalysts shown in Fig. 4b indicates a rather homogeneous distribution of Fe on the surface of our catalysts and, therefore, the existence of lateral interactions that would inhibit OH adsorption on Pt atoms. However, the composition effects presented in Fig. 6 cannot be explained in terms of reduced OH coverage on Pt sites alone. In fact, as the Fe content gets larger the OH adsorption on Pt sites is increasingly inhibited but the number of Pt sites available on the surface decreases. Consequently, the larger ORR activities observed for PtFe/C catalysts of compositions Pt:Fe 80:20 and

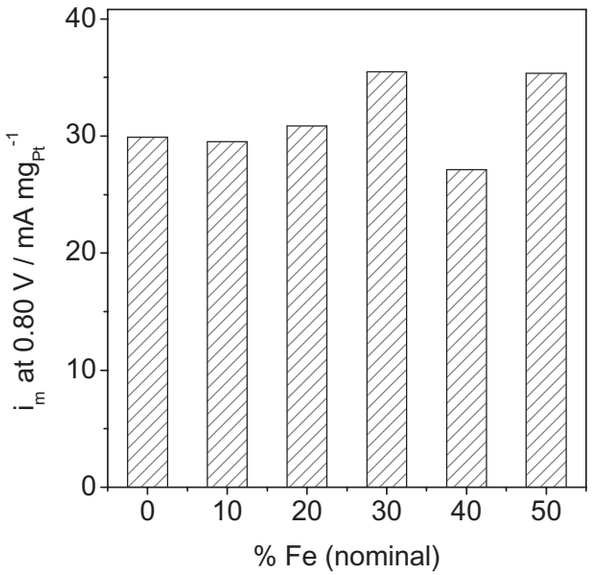

Figure 8. Pt mass-normalized ORR current densities measured at 0.80 V in the presence of 0.1 mol L^{-1} methanol against catalyst nominal Fe content (in atoms).

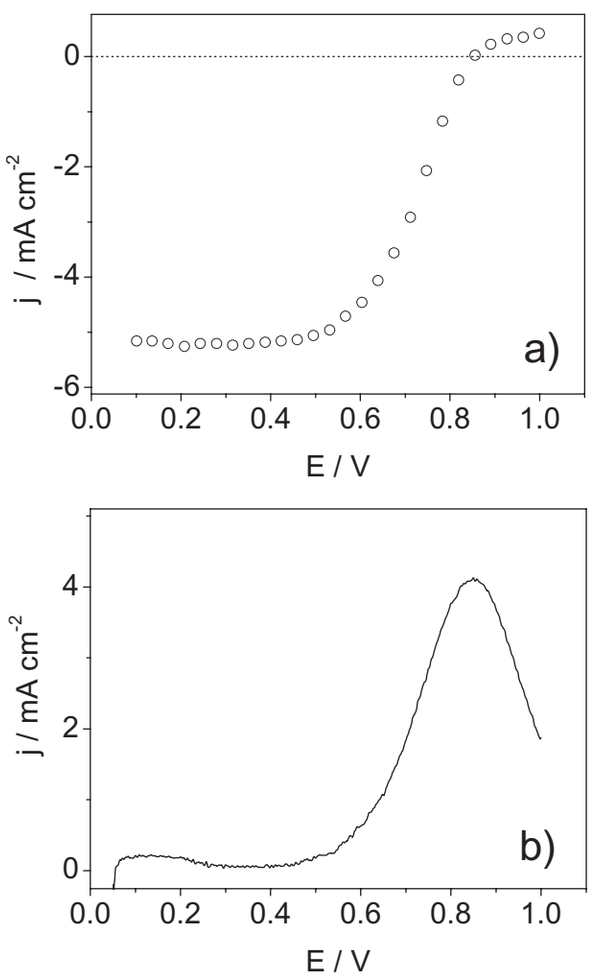

Figure 9. (a) ORR polarization curve of the PtFe/C 80:20 taken in O_2-saturated 0.1 mol L^{-1} of methanol +0.5 mol L^{-1} H_2SO_4 acid solution. Sweep rate: 5 mV s^{-1}, rotation rate: 2500 rpm. (b) Linear sweep voltammetry curves for methanol oxidation obtained in N_2-saturated solution (0.1 mol L^{-1} of methanol + 0.5 mol L^{-1} H_2SO_4). Sweep rate: 50 mV s^{-1}.

70:30 would result of the opposite effects on ORR activity of the number and OH coverage of Pt sites, as suggested by Nilekar et al.[61]

ORR in the presence of methanol.— Pt/C electrocatalysts suffer severe losses of performance for the ORR in the presence of methanol caused by the crossover of the alcohol through the proton exchange membrane. Thus, methanol-tolerant catalysts for ORR are needed to improve the performance of direct methanol fuel cells. Pt mass-normalized ORR current densities measured at 0.80 V and 2500 rpm in the presence of 0.1 mol L^{-1} methanol are shown in Fig. 8 against catalyst composition. In general, PtFe/C catalysts have a similar or better ORR performance than Pt/C in the presence of methanol, depending on their composition.

Shukla et al.[6] compared a PtFe/C catalyst of nominal composition 50:50 with Pt/C by doing cyclic voltammetry in O_2-free methanol-containing solutions, and concluded that methanol oxidation was less favored on PtFe/C. Moreover, when the same catalysts were used as cathodes (with the same Pt load) in a 4 cm^2 direct methanol fuel cell at 85°C, they observed higher power densities for the bimetallic material and concluded that PtFe/C was more tolerant to methanol than Pt/C.

However, for the PtFe/C nanocatalysts prepared in this work, the polarization curves for the ORR taken in the presence of 0.1 mol L^{-1} methanol show that positive currents are measured above ca. 0.85 V, as shown in Fig. 9a for PtFe/C 80:20. This indicates that the PtFe/C catalysts are active toward methanol oxidation. Figure 9b depicts, as an example, the curve of methanol oxidation in the absence of O_2 for the PtFe/C nanocatalyst of composition 80:20. In a general manner, all catalysts studied in this work exhibited similar behavior. A comparison of ORR current densities measured at 0.80 V and ω = 2500 rpm in the absence and in the presence of methanol is shown in Fig. 10.

The presence of methanol produced losses of about 40% of the current for Pt/C and PtFe/C catalysts of compositions 90:10 and 60:40. Larger losses are observed for PtFe/C nanocatalysts of composition 80:20 and 70:30, while for PtFe/C 50:50 the current drop is less than 20%. These data indicate that, even though larger ORR currents and mass activities might be measured on PtFe/C catalysts, their methanol tolerance is only apparent.

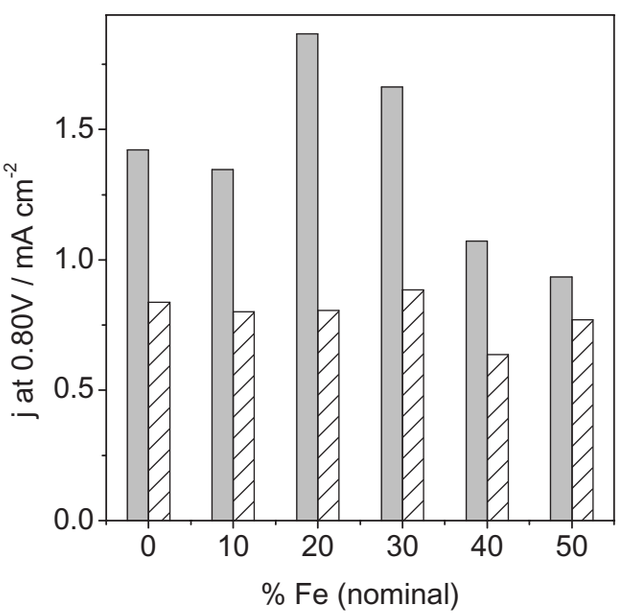

Figure 10. Current densities of ORR at 0.80 V against Fe nominal content (in atoms) in the absence of methanol (gray) and in methanol-containing solution (dashed). Rotation rate: 2500 rpm.

Conclusions

We have demonstrated that PtFe/C nanocatalysts prepared in AOT + *n*-butanol/*n*-heptane/water microemulsions are well-alloyed, and that both Pt and Fe are present on the surface. We have also shown that these nanocatalysts can be obtained with different compositions and the same particle size, and that they are monodispersed. PtFe/C nanocatalysts exhibit ORR activities that depend on composition and that are superior to that of Pt/C. The larger activity for ORR observed for catalysts of compositions Pt:Fe 80:20 and 70:30 would result from the combined effects of the number of Pt sites and their OH coverage. Even though the PtFe/C nanocatalysts do not seem to be really tolerant to the presence of methanol, they exhibit similar or better ORR performance than Pt/C in the presence of methanol, depending on their composition. The use of these catalysts as cathode materials in PEMFCs could allow decreasing the Pt load while improving cell performance.

Acknowledgments

Thanks are due to the Brazilian Agencies Fundação de Amparo à Pesquisa do Estado de São Paulo (FAPESP, 04/15570-8; 07/54434-0), Conselho Nacional de Desenvolvimento Científico e Tecnológico (CNPq, 480662/2007-0), and Financiadora de Estudos e Projetos (FINEP 01.06.0939.00) for financial support. A.R.M. and J.P. thank CNPq for the fellowships granted.

FAPESP assisted in meeting the publication costs of this article.

References

1. H. A. Gasteiger, W. Gu, R. Makharia, M. F. Mathias, and B. Sompalli, in *Handbook of Fuel Cells: Fundamentals, Technology, and Applications*, Vol. 3, W. Vielstich, A. Lamm, and H. A. Gasteiger, Editors Chap. 46, p. 593, John Wiley & Sons, New York (2003).
2. S. Mukerjee, S. Srinivasan, M. P. Soriaga, and J. McBreen, *J. Electrochem. Soc.*, **142**, 1409 (1995).
3. T. Toda, H. Igarashi, and M. Watanabe, *J. Electroanal. Chem.*, **460**, 258 (1999).
4. T. Toda, H. Igarashi, H. Uchida, and M. Watanabe, *J. Electrochem. Soc.*, **146**, 3750 (1999).
5. L. Xiong, A. M. Kannan, and A. Manthiram, *Electrochem. Commun.*, **4**, 898 (2002).
6. A. K. Shukla, R. K. Raman, N. A. Choudhury, K. R. Priolkar, P. R. Sarode, S. Emura, and R. Kumashiro, *J. Electroanal. Chem.*, **563**, 181 (2004).
7. W. Li, W. Zhou, H. Li, Z. Zhou, B. Zhou, G. Sun, and Q. Xin, *Electrochim. Acta*, **49**, 1045 (2004).
8. V. S. Murthi, R. C. Urian, and S. Mukerjee, *J. Phys. Chem. B*, **108**, 11011 (2004).
9. L. Xiong and A. Manthiram, *J. Electrochem. Soc.*, **152**, A697 (2005).
10. L. Xiong and A. Manthiram, *Electrochim. Acta*, **50**, 2323 (2005).
11. M. Teliska, V. S. Murthi, and S. Mukerjee, *J. Electrochem. Soc.*, **152**, A2159 (2005).
12. W. Yuan, K. Scott, and H. Cheng, *J. Power Sources*, **163**, 323 (2006).
13. A. Stassi, C. D'Urso, V. Baglio, A. Di Blasi, V. Antonucci, A. S. Arico, A. M. Castro Luna, A. Bonesi, and W. E. Triaca, *J. Appl. Electrochem.*, **36**, 1143 (2006).
14. H. Yano, M. Kataoka, H. Yamashita, H. Uchida, and M. Watanabe, *Langmuir*, **23**, 6438 (2007).
15. Y. Gong, Y. D. Yeboah, S. N. Lvov, V. Balashov, and Z. Wang, *J. Electrochem. Soc.*, **154**, B560 (2007).
16. V. Stamenkovic, T. J. Schmidt, P. N. Ross, and N. M. Markovic, *J. Electroanal. Chem.*, **554**, 191 (2003).
17. H. Yang, W. Vogel, C. Lamy, and N. Alonso-Vante, *J. Phys. Chem. B*, **108**, 11024 (2004).
18. T. C. Deivaraj and J. Y. Lee, *J. Electrochem. Soc.*, **151**, A1832 (2004).
19. H. Yang, C. Coutanceau, J.-M. Leger, N. Alonso-Vante, and C. Lamy, *J. Electroanal. Chem.*, **576**, 305 (2005).
20. E. Antolini, J. R. C. Salgado, A. M. dos Santos, and E. R. Gonzalez, *Electrochem. Solid-State Lett.*, **8**, A226 (2005).
21. U. A. Paulus, A. Wokaun, G. G. Scherer, T. J. Schmidt, V. Stamenkovic, V. Radmilovic, N. M. Markovic, and P. N. Ross, *J. Phys. Chem. B*, **106**, 4181 (2002).
22. V. Stamenkovic, T. J. Schmidt, P. N. Ross, and N. M. Markovic, *J. Phys. Chem. B*, **106**, 11970 (2002).
23. M. Min, J. Cho, K. Cho, and H. Kim, *Electrochim. Acta*, **45**, 4211 (2000).
24. M. D. Obradovic, B. N. Grgur, and L. M. Vracar, *J. Electroanal. Chem.*, **548**, 69 (2003).
25. U. Koponen, H. Kumpulainen, M. Bergelin, J. Keskinen, T. Peltonen, M. Valkiainen, and M. Wasberg, *J. Power Sources*, **118**, 325 (2003).
26. J. R. C. Salgado, E. Antolini, and E. R. Gonzalez, *J. Electrochem. Soc.*, **151**, A2143 (2004).
27. J. R. C. Salgado, E. Antolini, and E. R. Gonzalez, *J. Power Sources*, **138**, 56 (2004).
28. J. R. C. Salgado, E. Antolini, and E. R. Gonzalez, *J. Phys. Chem. B*, **108**, 17767 (2004).
29. J. R. C. Salgado, E. Antolini, and E. R. Gonzalez, *J. Power Sources*, **141**, 13 (2005).
30. E. Antolini, J. R. C. Salgado, M. J. Giz, and E. R. Gonzalez, *Int. J. Hydrogen Energy*, **30**, 1213 (2005).
31. J. N. Soderberg, A. H. C. Sirk, S. A. Campbell, and V. I. Birss, *J. Electrochem. Soc.*, **152**, A2017 (2005).
32. Y. Takasu, R. Matsuyama, S. Konishi, W. Sugimoto, and Y. Murakami, *Electrochem. Solid-State Lett.*, **8**, B34 (2005).
33. E. I. Santiago, L. C. Varanda, and H. M. Villullas, *J. Phys. Chem. C*, **111**, 3146 (2007).
34. M. Neergat, A. K. Shukla, and K. S. Gandhi, *J. Appl. Electrochem.*, **31**, 3373 (2001).
35. H. Yang, N. Alonso-Vante, J. M. Leger, and C. Lamy, *J. Phys. Chem. B*, **108**, 1938 (2004).
36. J.-M. Leger, *Electrochim. Acta*, **50**, 3123 (2005).
37. H. Yang, N. Alonso-Vante, C. Lamy, and D. L. Akins, *J. Electrochem. Soc.*, **152**, A704 (2005).
38. E. Antolini, J. R. C. Salgado, L. G. R. A. Santos, G. Garcia, E. A. Ticianelli, E. Pastor, and E. R. Gonzalez, *J. Appl. Electrochem.*, **36**, 355 (2006).
39. G. Cambanis and D. Chadwick, *Appl. Catal.*, **25**, 191 (1986).
40. E. Antolini, R. R. Passos, and E. A. Ticianelli, *Electrochim. Acta*, **48**, 263 (2002).
41. E. Antolini, *J. Appl. Electrochem.*, **137**, 563 (2004).
42. A. R. Malheiro, J. Perez, and H. M. Villullas, *ECS Trans.*, **6**(25), 85 (2008).
43. A. R. Malheiro, L. C. Varanda, J. Perez, and H. M. Villullas, *Langmuir*, **23**, 11015 (2007).
44. J. Schmidt, H. A. Gasteiger, G. D. Stab, P. M. Urban, D. M. Kolb, and R. J. Behm, *J. Electrochem. Soc.*, **145**, 2354 (1998).
45. B. C. Cullity, *Elements of X-ray Diffraction*, 2nd ed., p. 555, Addison-Wesley Publishing Company, Inc., London (1978).
46. E. Antolini, J. R. C. Salgado, and E. R. Gonzalez, *J. Electroanal. Chem.*, **580**, 145 (2005).
47. R. J. Hunter, *Foundations of Colloid Science*, Vol. 1, p. 104, Clarendon Press, Oxford (1989).
48. W. H. Lizcano-Valbuena, V. A. Paganin, C. A. P. Leite, F. Galembeck, and E. R. Gonzalez, *Electrochim. Acta*, **48**, 3869 (2003).
49. U. A. Paulus, A. Wokaun, G. G. Scherer, T. J. Schmidt, V. Stamenkovic, N. M. Markovic, and P. N. Ross, *Electrochim. Acta*, **47**, 3787 (2002).
50. B. E. Conway and G. Jerkiewicz, *Electrochim. Acta*, **45**, 4075 (2000).
51. J. Perez, E. R. Gonzalez, and E. A. Ticianelli, *Electrochim. Acta*, **44**, 1329 (1998).
52. U. A. Paulus, T. J. Schmidt, H. A. Gasteiger, and R. J. Behm, *J. Electroanal. Chem.*, **495**, 134 (2001).
53. M. R. Tarasevich, A. Sadkowski, and E. Yeager, in *Comprehensive Treatise in Electrochemistry*, J. O. M. Bockris, B. E. Conway, E. Yeager, S. U. M. Khan, and R. E. White, p. 301, Plenum, New York (1983).
54. J. Perez, H. M. Villullas, and E. R. Gonzalez, *J. Electroanal. Chem.*, **435**, 179 (1997).
55. L. G. R. A. Santos, C. H. F. Oliveira, I. R. Moraes, and E. A. Ticianelli, *J. Electroanal. Chem.*, **596**, 141 (2006).
56. K. Kinoshita, *J. Electrochem. Soc.*, **137**, 845 (1990).
57. K. Kinoshita, *Electrochemical Oxygen Technology*, John Wiley & Sons, New York (1992).
58. R. R. Adzic, in *Electrocatalysis (Frontiers in Electrochemistry)*, J. Lipkowski and P. N. Ross, Editors, p. 197, John Wiley & Sons, New York (1998).
59. V. Jalan and E. J. Taylor, *J. Electrochem. Soc.*, **130**, 2299 (1983).
60. J. X. Wang, N. M. Markovic, and R. R. Adzic, *J. Phys. Chem. B*, **108**, 4127 (2004).
61. A. U. Nilekar, Y. Xu, J. Zhang, M. B. Vukmirovic, K. Sasaki, R. R. Adzic, and M. Mavrikakis, *Top. Catal.*, **46**, 276 (2007).